INSTITUTE OF PHYSICS PUBLISHING JOURNAL OF PHYSICS B: ATOMIC, MOLECULAR AND OPTICAL PHYSICS

J. Phys. B: At. Mol. Opt. Phys. **39** (2006) 719–728 doi:10.1088/0953-4075/39/3/023

Differential cross sections for excitation to the 3s, 3p and 3d states of atomic hydrogen by electron impact at energies from 16.5 to 54 eV

J F Williams[1], Philip L Bartlett[2], Igor Bray[2], Andris T Stelbovics[2] and A G Mikosza[1]

[1] Centre for Atomic, Molecular and Surface Physics, University of Western Australia, Perth WA 6009, Australia
[2] Centre for Atomic, Molecular and Surface Physics, Murdoch University, Perth WA 6150, Australia

Received 24 October 2005, in final form 6 December 2005
Published 9 January 2006
Online at stacks.iop.org/JPhysB/39/719

Abstract

The excitation of atomic hydrogen from the ground state to each of the 3s, 3p and 3d states has been studied for incident electron energies from 16.5 to 54 eV. Measurements of total cross sections and differential excitation cross sections (DCSs) for scattered electron angles from 5° to 150° have been made using a variety of coincidence methods. Within the summed experimental uncertainties of about 10% at best from statistical sources and 25% from absolute calibration sources the values calculated using the propagating exterior complex scaling and convergent close-coupling methods show good agreement with observations. DCS calculations for all s, p, d and f final states with $n \leqslant 4$ are also presented over this energy range and reveal a systematic trend with respect to increasing n, final-state angular momentum and incident energy.

(Some figures in this article are in colour only in the electronic version)

1. Introduction

This paper concerns primarily the measurement of the total and differential cross sections for electron-impact excitation of the separate 3s and 3d angular momentum states of atomic hydrogen which has not been reported previously. The work is part of the general programme to characterize the separated angular momentum states and their magnetic sublevels as well as their electron–photon angular and polarization correlations. It is expected that these correlation quantities may reveal aspects of the collision process that otherwise may not be evident or are not well described in the total and differential cross sections when summed over the separate states. The renewed interest in this three-body scattering problem arises from recent experimental and theoretical advances described in the next paragraph.

A new apparatus and a new technique, of physically moving the incident atomic beam in and out of the observed designated interaction region, have demonstrated an improved signal-to-noise ratio with consequent improved precision and accuracy of measurements (James *et al* 2004) at least for non-coincidence techniques. These developments led to the measurement of the ratios of differential cross sections for excitation to the $n = 2$, 3 and 4 levels at energies from 14.6 to 40 eV (James *et al* 2004); their values support earlier $n = 2$ measurements (Williams and Willis 1975, Williams 1981, Slevin 1984) as well as providing new data for the $n = 3$ and 4 levels. Their approach and cross section calibrations were established by two supporting measurements of (i) new double angular differential ionization cross sections from 14.6 to 40 eV (Childers *et al* 2003, 2004) and (ii) differential elastic scattering cross section measurements at 20 and 40 eV (James *et al* 2004). The latter also supported earlier measurements (Callaway and Williams 1975). In summary, the agreement is generally within plus/minus one standard deviation that varies from about 8% to 18% of the cross section values which range from about 10^{-20} cm^2 sr^{-1} for 40 eV excitation of the total $n = 4$ states and from about 10^{-19} cm^2 sr^{-1} eV for DDCS ionization.

However, for measurements of the $n = 3$, 4 and higher levels, major experimental difficulties arise from the energy degeneracy of the states and cascade transitions. Neither electron energy loss spectroscopy nor photon spectroscopy alone permits separation of the $n = 3$ angular momentum levels. Only the total $n = 3$ cross section measurements of Mahan *et al* (1976) have used a technique which modulated the electron beam and separated the states via their different lifetimes; the subsequent use of the method has not been reported presumably because of its limited applicability. Consequently, the experimental approach has been to detect in coincidence the scattered energy-loss electrons with the radiated photons. This introduced the possibility of obtaining information about the initially excited 3s and 3d states by observing the cascade Lyman-alpha photons emitted from the intermediate 2p states (Chwirot and Slevin 1987a, Williams *et al* 1993a, 1993b) in coincidence with the $n = 3$ energy-loss electrons. Measurements of the differential cross section for the 3p state at 54 eV were made by Williams *et al* (1993a, 1993b) together with measurements of the angular and polarization correlations for the 3p state at 54 eV (Williams *et al* 1993a, 1993b) and the circular polarization of the 3^2D_j states (Kumar *et al* 1993, Chwirot and Slevin 1987b, Farrell *et al* 1990). The notable feature of such measurements is that, while they are straightforward in principle, a relatively complex apparatus can be operated to give a reliable identification of the angular momentum states. Nevertheless, because these coincidence measurements require the use of at least two detectors the associated experimental precision and accuracy will not be better than measurements using only a single detector.

The present studies present absolute differential cross sections (DCS) for excitation from the ground state to the separate 3s, 3p and 3d states for scattered electron angles from 5° to 150° and for incident energies of 16.5, 19.6 and 54 eV. This spans the region of low impact energies, where large grids or basis sets are generally required for accurate calculations, to intermediate energies where an increasing number of partial waves make calculations more difficult. The measured values are compared with values from two state-of-the-art methods, propagating exterior complex scaling (PECS) (Bartlett *et al* 2004) (based on the exterior complex scaling method of Rescigno *et al* (1999)) and convergent close-coupling (CCC) (Bray and Stelbovics 1992).

2. Experimental details

The apparatus and experimental methods have been described in a series of papers (Williams *et al* 1993a, 1993b and references therein). Some essential details and modifications

are given here. The apparatus is based on a crossed electron–atom beams' geometry and uses the detection in coincidence of the scattered energy-loss electrons and the radiated photons from the decay of the excited state. The hydrogen atoms effuse from a 0.5 mm diameter Teflon tube (Williams *et al* 1993a, 1993b), whose outer surface is coated with conductive graphite and whose tip is 3 mm from the interaction region with a target density estimated to be of the order of 10^{11} to 10^{12} atoms cm^{-3}. The emergent beam is chopped at 117 Hz to modulate beam and background signals. For the present study, the electron beam current is typically several μA at 54 eV with a cross section of 1 mm^2, an angular spread of about 1° and an electron energy spread selected for the present measurements by a cylindrical electrostatic 127° analyser of 0.5 eV.

The scattered electrons are selected into a solid angle of about 5×10^{-2} sr; then focused into an energy analyser and subsequently detected by a microchannel plate electron multiplier. A 127° electron energy analyser is used to take advantage of its cylindrical symmetry about an axis normal to the scattering plane. Then the resolution of the scattering angle is chosen appropriately to reveal the angular variation of the differential cross section, i.e. at backward angles an angular resolution of 4° was used whereas at small forward angles a resolution of 1° was used. This required the inconvenience of opening the vacuum system to physically change the slit dimensions of the analyser and to have overlapping angular scans. However the advantage was that, where the cylindrical symmetry of the scattering geometry could be used, the azimuthal angle could be increased to at least 10° without introducing additional uncertainty into the measurements.

Photons are selected by a cone of large solid angle that was determined to optimize the measurement, as explained shortly. The 656.2 nm photons were detected by an EMI 9883 photomultiplier tube and the Lyman photons by a microchannel plate stack with appropriate filters. The resultant electron and photon pulses are amplified, discriminated and used to 'start and stop' a time-to-pulse-height analyser and recorded. Many tests have been made to ensure the validity of the measurements (Williams 1981 and references therein) and all of those tests are routinely repeated to ensure the reliability, precision and absolute accuracy of the cross sections.

However, the major advances of this paper which distinguish the work from earlier measurements concern the technical challenges of identifying the signals from the 3s, 3p and 3d states. It is straightforward to separate the $n = 2$, 3 and 4 energy-loss electrons in a rotatable 127° electron energy analyser. The correct use and location of the beam chopper and atomic hydrogen source ensure that the molecular hydrogen signals and elastically scattered electron signals are well identified. Williams *et al* (1993a, 1993b) gave the details for the identification of the 3p signals, particularly the use of an indium ultra-thin film low-pass 102.6 nm wavelength filter which blocked the 121.6 nm photons. Kumar *et al* (1993) described the identification of the 3d level via the coincidence detection of the cascade Lyman-alpha photons in coincidence with $n = 3$ energy-loss electron and in anti-coincidence with the $n = 2$ energy-loss electrons to reduce the directly excited Lyman-alpha photons. The separation of the 3s component was made via the lifetimes of 158, 5.3 and 15.5 ns of the 3s, 3p and 3d levels, respectively, for which the $n = 3$ energy-loss electrons provided the time-zero reference for the photon decay. These aspects of the measurements require extreme care and optimization of related experimental parameters in order to separate the 3s, 3p and 3d signals. The measurements were facilitated by using an appropriate solid angle of the photon detectors and locating them so that their count rates were independent of the averaged photon polarization.

The appearance energies of the photon signals also enabled the usefulness of the filters to be checked. For UV photon detection from the '*n*p' levels with electron incident energies

near threshold, at 10.0 eV there is only background molecular radiation, at 11.0 eV only Lyman-alpha photons and at 12.4 eV both Lyman-alpha and Lyman-beta photons. The 2p and 3p excitation thresholds were seen clearly and the relative values of Lyman-alpha to Lyman-beta transmissions measured.

The effectiveness of the anti-coincidence gate (the $n = 2$ energy-loss electrons, collected from $+10^\circ$ to -10°) on the Lyman-alpha photons to veto a significant fraction of directly excited 2p decay photons were best shown at 290 eV incident electron energy. There the 2p cross section is about 50 times the 3p cross section and the 2p differential cross section is strongly peaked in the forward direction. These 'vetoed photons' otherwise contributed a significant fraction of the random coincidence signal.

A useful check on the correct operation of the photon detectors was to measure the photon count rates also at 290 eV which are then approximately equal to the first Born approximation predictions with the ratios Q(3S):Q(3P):Q(3D):Q(2P):Q(2S) = 0.004 05:0.0618:0.003 03: 0.370:0.022$\left[\pi a_0^2\right]$ = 4:62:3:370:22. Since the branching ratios are $\gamma(3S \rightarrow 2P) = 1$, $\gamma(3D \rightarrow 2P) = 1$, $\gamma(3P \rightarrow 2S) = 0.112$ and $\gamma(3P \rightarrow 1S) = 0.88$, then the total cross sections are in the ratios of Q(2P):Q(2S):Q(3S) + Q(3D):Q(3P − 2S) = 55/3/1/1.

The total 3p cross section was measured by collecting the Lyman-beta photons either normal to the scattering plane or at 54.5° in the scattering plane where the photon intensity is independent of the polarization and directly proportional to the total cross section. The Balmer-alpha photons were collected with a parabolic mirror with a large solid angle of 1.2 sr and focused onto the EMI photomultiplier. The relative contributions from the 3s, 3p and 3d states were separated by their lifetimes and calibrated against the separately measured 3p total cross section.

The accuracy of the $n = 3$ lifetime measurements is dependent on the $n = 3$ excitation cross section which determines the count rate and hence the time required to acquire a given statistical accuracy. The excitation functions were calibrated via the 3p measurements, the ratio of inelastic to elastic data and the ratio of hydrogen to helium in the 'gas flow' method (Williams 1981) to give absolute cross sections. Detailed discussions of the experimental uncertainties have been given by Williams and Willis (1975) and Williams (1981). The total counting uncertainties were estimated from the dissociation fraction (3%), transmission fraction through the analyser (3%) and coincidence identification (8%) and in addition to the energy-dependent uncertainties for raw data statistics as shown in the figures for each datum point. In addition, the cross section calibrations contributed uncertainties from the elastic DCS calibration of 10%, the inelastic calibration of 12% and from the relative gas flow measurement of 3% to give a total average calibration uncertainty of 25%.

3. Calculations

PECS and CCC calculations for the total and differential scattering cross sections for electron-impact excitation of ground-state hydrogen to the 3s, 3p and 3d final states for incident energies of 16.5, 19.6 and 54 eV are presented for comparison with the experimental results. The PECS method is detailed in Bartlett and Stelbovics (2004a) and Bartlett *et al* (2004), and references therein. In summary, the PECS method directly and completely solves the non-relativistic time-independent Schrödinger equation for the scattering wavefunctions, in the coordinate space. Exterior complex scaling allows numerical solution on a finite grid without explicit knowledge of the boundary conditions at the edge of the grid, and scattering amplitudes are extracted from the scattering wavefunctions using a surface-integral method. The PECS method agrees well with other state-of-the-art computational methods and

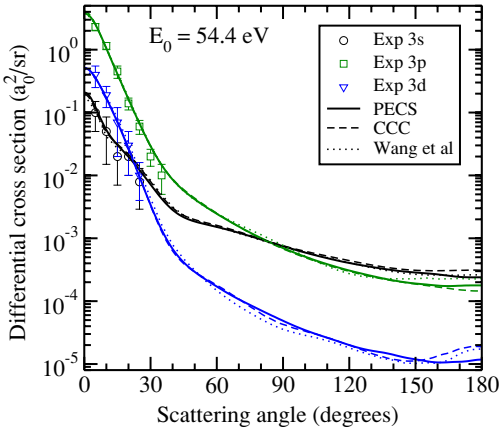

Figure 1. Differential cross section for excitation of the 3s, 3p and 3d levels of atomic hydrogen excited by 54.4 eV electrons. Present measurements: 3s circles, 3p squares, 3d diamonds; PECS calculations: 3s black, 3p green, 3d blue lines; CCC calculations: 3s black, 3p green, 3d blue dashed lines; Wang *et al* (1994) calculations: 3s black, 3p green, 3d blue dotted lines. Error bars show statistical uncertainty only.

measurements for both scattering and ionization over a broad range of energies (Bartlett and Stelbovics 2004b, Bartlett *et al* 2004, 2005).

The PECS calculations were undertaken for impact energies of 16.5, 19.6 and 54.4 eV with grid sizes of $R_0 = 100$, 80 and 80 au, respectively, and included partial waves with total angular momentum $L \leqslant 10$, 10 and 25, respectively. These partial waves were sufficient to obtain good convergence of the total scattering cross sections, though extrapolated scattering amplitudes for $L \leqslant 200$ were included to remove small oscillations in the differential cross sections in the highly suppressed back-scattering region. The estimated standard error of the 3s, 3p and 3d total scattering cross section calculations is 3%. DCS results are also calculated for the s, p, d and f states for all $n \leqslant 4$. The calculations have an increased estimated standard error for $n = 4$ total cross sections of 5%.

The details of the original Laguerre-based CCC method were given by Bray and Stelbovics (1992). Here, we use the box-based CCC method (Bray *et al* 2003) which has simpler foundations, but yields much the same results as the original method. The target discretization is obtained by imposing the boundary condition that the wavefunctions are zero at a specified radial value R_0. This value, the number of states N_l taken for each target-space orbital angular momentum l, and $l_{\max}$ define the target-space states used to expand the total wavefunction of the system. In the present case for the three incident energies of 16.5, 19.6 and 54.4 eV, the (R_0, N_l, $l_{\max}$) parameters were (80.0, 16 − l, 4), (80.0, 21 − l, 4) and (50.0, 20 − l, 4), respectively. The number of partial waves (L) treated explicitly increases with increasing energy. Once the Born approximation is sufficiently accurate, an analytic Born subtraction technique is used to sum the remaining partial-wave contribution, giving an effective extrapolation of L to infinity. The uncertainties in these CCC calculations, which arise mainly from varying minor pseudo-resonances, are of the order of 10%.

4. Results

Figures 1–3 show the angular differential cross sections at 54.4, 19.6 and 16.5 eV, respectively. At 54.4 eV ($k^2 = 4.0$) and 10° scattering angle, the 3s, 3p and 3d cross sections have values

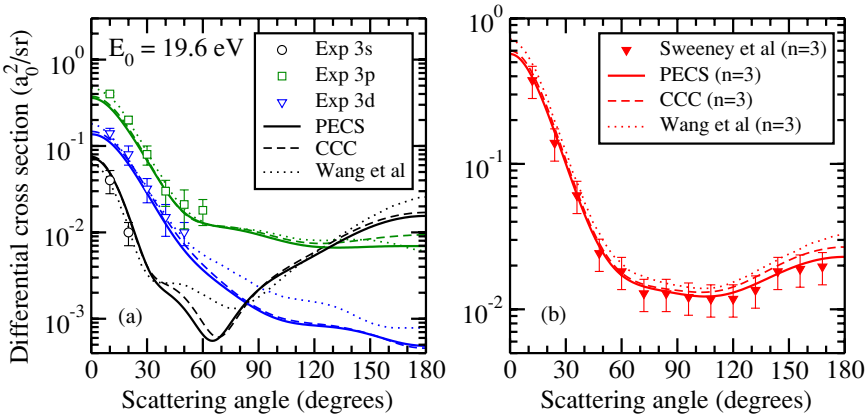

Figure 2. (a) The same as figure 1 at 19.6 eV. (b) Differential cross section for excitation to the $n = 3$ level at 19.6 eV. Sweeney *et al* (2001) measurements: triangles; PECS calculations: solid lines; CCC calculation: dashed lines; Wang *et al* (1994) calculations: dotted lines.

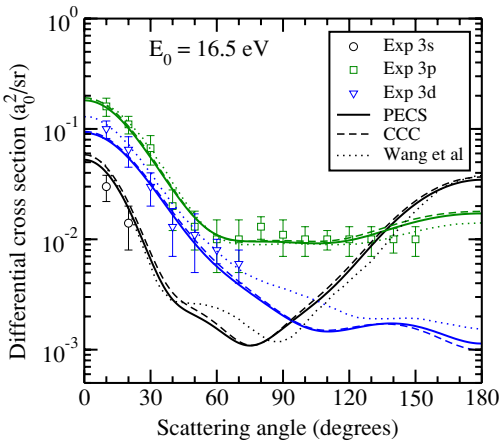

Figure 3. The same as figure 1 at 16.5 eV.

of 0.05, 1.1 and 0.2 a_0^2 sr^{-1}, respectively, and decrease rapidly with angle over the next 20°. The PECS, CCC and Wang *et al* (1994) calculations are in good agreement and contained within the statistical error bars of our measurements. The Wang *et al* (1994) calculations were obtained from a close-coupling calculation using a 17-state target basis that included seven exact states and ten pseudo-states.

At 19.6 eV ($k^2 = 1.44$ au) the 3s and 3p cross sections show strong forward and backward (up to 150°) scatterings while the 3d cross section decreases with increasing angle. The 3s cross section is small and the long lifetime limits the measurements. Two 3p data points at 10° and 20° deviate by more than two standard deviations (in the statistical error) from PECS and CCC calculations, yet are in good agreement with Wang *et al* (1994). Given that the 25% absolute calibration error is not included in the error bars, the present measurements cannot distinguish between the calculations. To explore further the variations in the calculations presented, we show the summed $n = 3$ PECS, CCC and Wang *et al* calculations in figure 2(b) along with the absolute 20 eV $n = 3$ measurements of Sweeney *et al* (2001) which have *total*

uncertainties of 25%. The PECS and CCC calculations are within all error bars and PECS appears to provide a slightly better fit in the back-scattering region. Unlike in the case of the individual components, here the Wang *et al* calculations are above the error bars at small scattering angles, where the cross sections are the largest. There is reasonably good agreement between the PECS and CCC calculations over most of the scattering angles, but they vary significantly from the Wang *et al* 3s and 3d calculations at the larger scattering angles where the cross section is too small to be measured.

At 16.5 eV ($k^2 = 1.21$ au) the 3p cross section at small angle scattering is decreasing relative to that at higher energies, and backward scattering has increased and allowed measurements up to 150°. The 3d cross section has increased to values similar to the 3p cross section. The lower limit of measurement was slightly less than $0.01a_0$ sr^{-1} which meant that the 3s cross sections could not be measured from about 30° to 120° and the 3d cross section could not be measured beyond 70°. Unfortunately at the time of the measurements it was not realized that the 3s cross section increased at large backward angles.

The calculations at 16.5 eV indicate that after 75° the 3s cross section increases rapidly and gives almost equal probability of forward and backward scatterings. Similar behaviour is observed at 19.6 eV. All calculations fall within the statistical error bars of our measurements, though the Wang *et al* (1994) close-coupling 3d calculations are consistently larger than the PECS and CCC calculations. As in the 19.6 eV calculations, there are larger discrepancies between the Wang *et al* calculations and the PECS and CCC calculations in the regions below the threshold of measurement.

The general behaviour of the differential cross sections is clear. At all energies and small angles, the 3p cross section is larger than the 3d which is larger than the 3s and all three become more strongly peaked in the forward direction as the incident electron energy increases. The 3d DCS falls off more rapidly than the 3p DCS but the 3s DCS shows the interesting behaviour of increasing at backward angles and doing so more strongly as the energy decreases until it becomes significantly larger than the 3p DCS near 180° at 16.5 eV. This behaviour of the 3s state DCS relative to the 2p DCS is somewhat reminiscent of the 2s DCS relative to the 2p DCS at 54.4 eV (Williams 1981).

In figure 4, we present PECS calculations (CCC are similar) for the DCS of all final states up to and including 4f at 16.5, 19.6 and 54.4 eV. These calculations enable an improved interpretation of the physical behaviour of the $n = 3$ cross sections. From the figures, we see a clear systematic trend with increasing incident energy and nl of the final state. First, we note that all inelastic scattering DCS curves have a small angular region where there is marked change in gradient of the curve. This separates small-angle scattering, which has a rapid attenuation with increasing scattering angle, from larger-angle scattering that has a more gradual reduction (or increase). This region is most evident in the s-state curves, but is present in all inelastic curves. In general, the scattering angle where this turning point occurs, increases with n, increases with l and reduces with increasing incident energy. Second, the magnitude of the DCS for inelastic scattering, decreases with increasing n, is the largest for p-states and decreases with increasing l, and in the larger-angle region the rate of attenuation increases with increasing energy and increases with l. Finally, we observe in the small-angle scattering region that the DCS is most sharply peaked at high energies and, with the exception of s-states, the slope is relatively independent of l.

The data are consistent with the phenomenological explanation that the collision mechanism involves small angle inelastic scattering and larger angle elastic scattering. For example, a simple physical model could involve the 16.5 eV incident energy losing 12.1 eV in the $n = 3$ excitation process, with a subsequent 4.4 eV elastic scattering which is known to have a large backward cross section up to about $3a_0^2$ sr^{-1} and a minimum cross section at

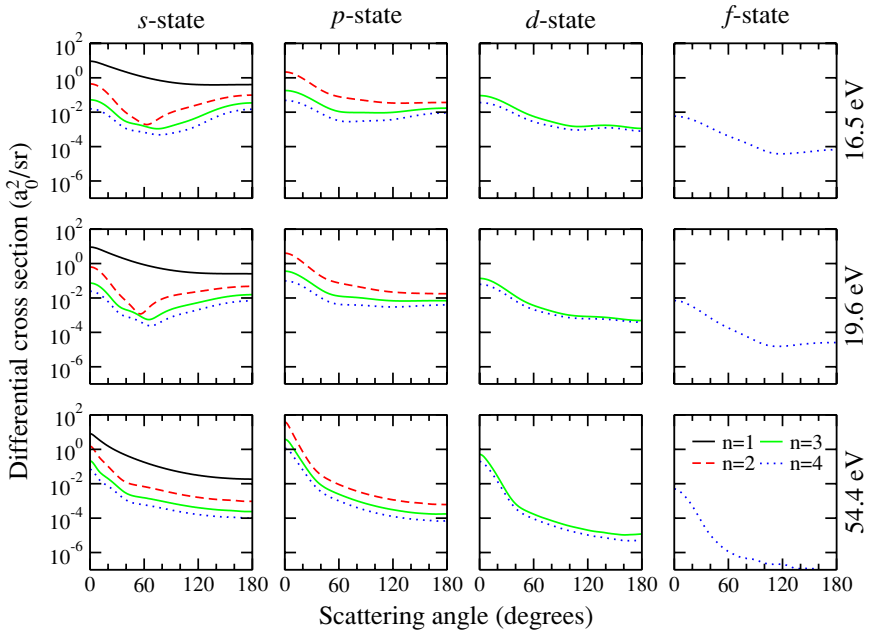

Figure 4. PECS differential cross section calculations for excitation of the s, p, d and f levels of atomic hydrogen with $n \leqslant 4$ by 16.5, 19.6 and 54.4 eV. Each column of plots represents different l-states; each row of plots represents different energies. Black solid lines, $n = 1$; red dashed lines, $n = 2$; light green solid lines, $n = 3$; blue dotted lines, $n = 4$.

about 70° (Williams 1975). If there was some mixing of this form of the elastic scattering following the excitation then the shape of the excitation DCS may be explained.

Figure 5 shows our total 3s, 3p and 3d cross section measurements. They are consistent, within the statistical uncertainties of one standard deviation of about 10% of the cross section values, with the data of Mahan *et al* (1976). At 54.4 eV our PECS and CCC calculations and the close-coupling calculations of Callaway and Unnikrishnan (1993) are in good agreement with our measurements. The Callaway and Unnikrishnan calculations used a 17-state basis set with seven exact (1s to 3d and 4f) and ten pseudo-states (5s-, 3p- and 2d-like), in a variational close-coupling calculation, and the pseudo-threshold structure in the continuum was removed by a fitting process. It is interesting to note, at least from an historical view, that with a reasonable set of carefully chosen pseudo-states it was possible to obtain cross sections at higher energies that are of similar accuracy to those obtained with our much larger discrete basis sets. At all energies the PECS and CCC total cross sections agree within their stated uncertainty; however near the threshold, the differences between the PECS and CCC calculations and the Callaway and Unnikrishnan calculations are as large as 30%. There is no systematic trend to the variances between the calculations and measurement, though all calculations are within the total uncertainty (10% statistical and 25% calibration) of our measurements.

Figure 6 shows the calculated partial-wave cross sections (PWCS) given as a percentage of the total cross section (TCS), for L up to 15, for the 3s, 3p and 3d total cross sections at 16.5 and 54 eV. They provide a ready interpretation of the observations. At both 16.5 and 54 eV the 3s DCS can be attributed almost entirely to partial waves of $L \leqslant 4$ whereas the 3p and 3d DCSs are progressively attributed to higher angular momentum effects with L important from

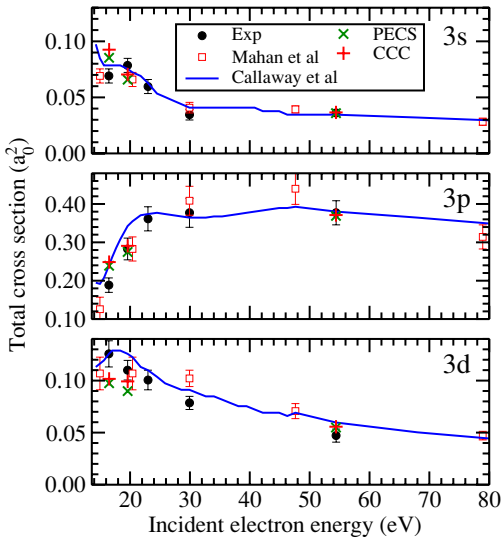

Figure 5. Summed cross sections for excitation of the 3s, 3p and 3d levels. Present measurements: filled circles; measurements of Mahan *et al* (1976): squares; ECS calculations: crosses; CCC calculations: pluses; Callaway and Unnikrishnan (1993) calculations: solid line. Error bars show statistical uncertainty only.

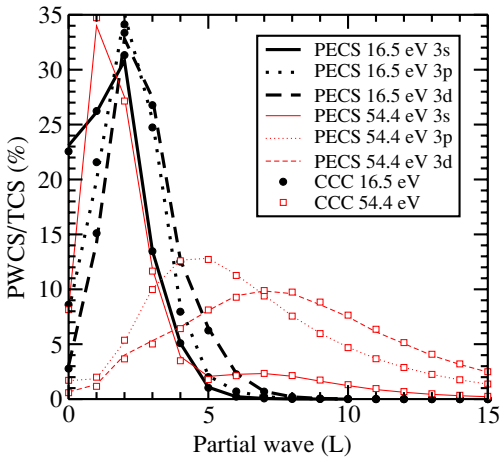

Figure 6. The calculated PECS and CCC partial-wave cross sections (PWCS) given as a percentage of total cross section (TCS), for L up to 15, are shown for the 3s, 3p and 3d total cross sections at 16.5 and 54 eV. The legend for PECS calculations is 3s (full line), 3p (dotted line) and 3d (dashed line) with fine red lines for the 54 eV data and thick black lines for the 16.5 data. CCC results: 16.5 eV, filled red circles; 54 eV, hollow red squares.

$L = 0$ up to approximately 15 and with maximum contributions at $L = 5$ and $L = 7$ to the 3p and 3d DCSs, respectively. The profile of the partial-wave contributions is consistent with expectations, where DCS curves with sharper peaks require more expansion terms to represent them accurately. Thus, as the rate of attenuation of small-angle scattering increases with energy, and the ratio of back-scattering to forward-scattering increases, a larger number of partial waves are required. Relative to higher angular momentum states, the s-state cross

sections are much flatter and continue to have a dominant small L contribution at high energies. Interestingly, the partial-wave contributions to the 54.4 eV 3s state has a double-peak structure with the primary peak at $L = 1$, of similar shape to the low-energy collision, and a secondary peak at $L = 7$, of similar shape to the 54.4 eV d-state collision.

5. Conclusions

The major result of this work is that a series of difficult measurements has led to observations of the angular differential cross sections for the excitation of the separated 3s, 3p and 3d states of atomic hydrogen. PECS calculations were also presented for all states with $n \leqslant 4$, which reveal the systematic change in the shape and magnitude of the DCS with respect to incident energy and final-state orbital and angular momentum. The observed values are in agreement within the large experimental uncertainties with the values calculated using the propagating exterior complex scaling (PECS) and convergent close-coupling (CCC) methods. The measurements confirm within about 35% the differential cross sections for excitation to the separate $n = 3$ states, originally calculated by Wang *et al* (1994) and now calculated using the PECS and CCC methods. A significant improvement in experimental method and reduction of uncertainties of measurement are required in order to differentiate between the calculations presented here.

References

Bartlett P L and Stelbovics A T 2004a *Phys. Rev.* A **69** 022703
Bartlett P L and Stelbovics A T 2004b *Phys. Rev. Lett.* **93** 233201
Bartlett P L, Stelbovics A T and Bray I 2004 *J. Phys. B: At. Mol. Opt. Phys.* **37** L69
Bartlett P L, Stelbovics A T, Lee G M and Bray I 2005 *J. Phys. B: At. Mol. Opt. Phys.* **38** L95
Bray I, Bartschat K and Stelbovics A T 2003 *Phys. Rev.* A **67** 060704(R)
Bray I and Stelbovics A T 1992 *Phys. Rev.* A **46** 6995
Callaway J and Unnikrishnan K 1993 *Phys. Rev.* A **48** 4292
Callaway J and Williams J F 1975 *Phys. Rev.* A **12** 2312
Childers J G, James K E, Bray I, Baertschy M and Khakoo M A 2004 *Phys. Rev.* A **69** 022709
Childers J G, James K E, Hughes M, Bray I, Baertschy M and Khakoo M A 2003 *Phys. Rev.* A **68** 030702(R)
Chwirot S and Slevin J 1987a *J. Phys. B: At. Mol. Phys.* **20** 3885
Chwirot S and Slevin J 1987b *J. Phys. B: At. Mol. Phys.* **20** 6139
Farrell D, Chwirot S, Srivastava R and Slevin J 1990 *J. Phys. B: At. Mol. Opt. Phys.* **23** 315
James K E, Childers J G and Khakoo M A 2004 *Phys. Rev.* A **69** 022710
Kumar M, Stelbovics A T and Williams J F 1993 *J. Phys. B: At. Mol. Opt. Phys.* **26** 2165
Mahan A H, Gallagher A and Smith S J 1976 *Phys. Rev.* A **13** 156
Rescigno T N, Baertschy M, Isaacs W A and McCurdy C W 1999 *Science* **286** 2474
Slevin J A 1984 *Rep. Prog. Phys.* **47** 461
Sweeney C J, Grafe A and Shyn T W 2001 *Phys. Rev.* A **64** 032704
Wang Y D, Callaway J and Unnikrishnan K 1994 *Phys. Rev.* A **49** 1854
Williams J F 1975 *J. Phys. B: At. Mol. Phys.* **8** 1683
Williams J F 1981 *J. Phys. B: At. Mol. Phys.* **14** 1197
Williams J F, Kumar M and Stelbovics A T 1993a *Phys. Rev. Lett.* **70** 1240
Williams J F, Stelbovics A T and Bray I 1993b *J. Phys. B: At. Mol. Opt. Phys.* **26** 4599
Williams J F and Willis B A 1975 *J. Phys. B: At. Mol. Phys.* **8** 1641